Carsten Seidel[1,*]

Daliborka Nikolić[2]

Matthias Felischak[3]

Menka Petkovska[4]

Andreas Seidel-Morgenstern[1,3]

Achim Kienle[1,3]

Forced Periodic Operation of Methanol Synthesis in an Isothermal Gradientless Reactor

Methanol synthesis from synthesis gas with heterogeneous Cu/ZnO/Al$_2$O$_3$ catalysts in an isothermal gradientless reactor is described. In a theoretical study, the potential of forced periodic operation (FPO) for improving reactor performance in terms of methanol production rate and methanol yield is explored. The approach is based on a detailed kinetic model and combines nonlinear frequency response (NFR) analysis with rigorous numerical multi-objective optimization. Optimal steady-state operation is compared with optimal forced periodic operation for a given benchmark problem with and without inert nitrogen in the feed. Further, the significant influence of the saturation capacity of the solid phase on the dynamic behavior in response to step changes and periodic input modulations is studied.

Keywords: Forced periodic operation, Methanol synthesis, Multi-objective optimization, Nonlinear frequency response, Pareto fronts

1 Introduction

Methanol is produced in large amounts from synthesis gas using heterogeneous catalysts [1]. In the context of numerous activities to exploit power and to store energy, there is currently increasing interest and demand for this alcohol [2, 3]. Various types of fixed-bed reactors are industrially applied to synthesize methanol [4]. Due to kinetic reasons, besides CO, also smaller amounts of CO$_2$ are present in the feed stream. The essential overall reactions are the hydrogenations of both CO and CO$_2$ and the reverse water-gas shift reaction. The reduction in the mole numbers and the thermodynamic properties of the components involved require operation at elevated pressure. Due to the strong exothermicity of the hydrogenation reactions, significant cooling is needed. The currently widely applied Cu/ZnO/Al$_2$O$_3$ catalysts are exploited at temperature between 220 and 270 °C and at pressures around 50 bar [2, 4].

Methanol synthesis reactors are currently designed to operate under steady-state conditions. In contrast, it is known that forced dynamic operation based on perturbing periodically certain input parameters possesses the potential for process improvements [5]. In the last years, the nonlinear frequency response (NFR) method [6, 7] and advanced multi-objective optimization tools [8, 9] have been developed, which support evaluating the potential of advanced forced periodic operation compared to traditional steady-state operation. An important recent result is the fact that it is very attractive to perturb two inputs simultaneously and to exploit a phase shift between these perturbations as an additional degree of freedom [10].

The key ingredient required to apply these theoretical concepts is the availability of a validated and sufficiently accurate dynamic process model. Considering the heterogeneously catalyzed methanol synthesis, a process model must consist of two equally challenging submodels. At first, there is a model needed that describes the rates of the reactions on the surface of the catalyst in the parameter space relevant for the periodic regime considered. This model needs to be combined with a reactor model that describes the concentration and temperature fields in the reactor of interest.

In this paper, we rely on the results of an extensive earlier experimental study on the steady state as well as dynamic transient behavior using a commercial Cu/ZnO/Al$_2$O$_3$ catalyst [11].

---

[1]Carsten Seidel (ORCID) https://orcid.org/0000-0003-0870-3651,
Prof. Andreas Seidel-Morgenstern, Prof. Achim Kienle
(carsten.seidel@ovgu.de)
Otto-von-Guericke University, Universitaetsplatz 2, 39106 Magdeburg, Germany.

[2]Daliborka Nikolić
University of Belgrade, Institute of Chemistry, Technology and Metallurgy, Njegoseva 12, 11000 Belgrade, Serbia.

[3]Dr. Matthias Felischak, Prof. Andreas Seidel-Morgenstern, Prof. Achim Kienle
Max-Planck-Institut für Dynamik komplexer technischer Systeme, Sandtorstr. 1, 39106 Magdeburg, Germany.

[4]Dr. Menka Petkovska
University of Belgrade, Faculty of Technology and Metallurgy, Department of Chemical Engineering, Karnegijeva 4, 11000 Belgrade, Serbia.

Wiley Online Library

To generate well-defined results and to simplify the reactor model required to analyze the results, methanol synthesis was performed in a gradientless reactor of the Berty type [12, 13] under isothermal and isobaric conditions. In these experiments, CO was the main carbon source, complemented by minor amounts of CO_2. The additional application of an inert gas in the feed (nitrogen) allowed measuring the degree of gas contraction. The large data set generated was of high quality and fulfilled the mass balances of all compounds involved very well [11]. A more recently performed deeper analysis of the available data led to the formulation and successful parameterization of a kinetic model [14, 15], which describes the data and provides the basis for the present work.

In this paper, the potential of forced periodic operation of methanol synthesis is studied theoretically using the NFR method and multi-objective optimization. For simplicity, an isothermal isobaric continuous stirred-tank reactor (CSTR) is considered representing a Berty type of reactor. The present paper extends the results in [16–18]. In [17], it was shown for a given benchmark problem that up to 33.51 % improvement of the methanol flow rate is possible in forced periodic operation compared to steady-state operation, if the focus is only on this objective.

It was shown in [17, 18] that methanol flow rate and methanol yield based on total carbon in the feed can be improved simultaneously if multi-objective optimization is applied. For multi-objective optimization, maximum improvement of the methanol flow rate was approximately 27 %, and maximum improvement of the yield was about 4 % [17] for a given operating point on the Pareto front. Results were obtained for simultaneous forcing of CO in the feed and the total volumetric feed flow rate, which was found most promising. According to [11], a mean value 15 % of nitrogen in the feed was considered. In the present paper, the optimization methodology introduced in [18] is extended. As a consequence, additional solution branches are found for the case with inert nitrogen. In addition, also industrially more relevant cases without inert nitrogen are considered.

2 Theoretical Methods

2.1 Kinetic Model

The calculations in this paper are based on the lumped kinetic model for the three essential reactions which take place in the heterogeneously catalyzed synthesis of methanol from synthesis gas. Details of this model are presented in [14, 15] with readjusted parameters from [16, 18] using the comprehensive set of steady-state and dynamic experimental data from [11]. These data were obtained over a wide range of operating conditions in a micro Berty reactor using a commercial Cu/ZnO/Al_2O_3 catalyst in the presence of 15 % of nitrogen in the feed gas used to quantify the degree of contraction. The model accounts for hydrogenation of CO and CO_2 and the reverse water-gas shift reaction according to:

$$CO + 2H_2 \rightleftharpoons CH_3OH \tag{1}$$

$$CO_2 + 3H_2 \rightleftharpoons CH_3OH + H_2O \tag{2}$$

$$CO_2 + H_2 \rightleftharpoons CO + H_2O \tag{3}$$

The lumped kinetic model assumes a Langmuir-Hinshelwood mechanism comprising the adsorption of reactants, surface reaction, and desorption of products. Adsorption and desorption are assumed to be in quasistatic equilibrium, which seems reasonable in view of the time constants of the dynamic processes to be considered subsequently, which lie in the range of 10 s with inert nitrogen up to 10 min without inert nitrogen.

The model assumes that there are three different active sites on the catalyst surface, namely:
- oxidized sites $\odot$ for CO hydrogenation,
- reduced sites * for CO_2 hydrogenation,
- and active sites $\otimes$ for heterolytic water decomposition.

The resulting expressions for the reactions rates r[1] are:

$$r_{CO} = (1 - \phi)k_1\left(p_{CO}p_{H_2}^2 - \frac{p_{CH_3OH}}{K_{P1}}\right)\theta^\odot\theta^{\otimes^4} \tag{4}$$

$$r_{CO_2} = \phi^2 k_2\left(p_{CO_2}p_{H_2}^2 - \frac{p_{CH_3OH}p_{H_2O}}{K_{P2}\,p_{H_2}}\right)\theta^{*2}\theta^{\otimes^4} \tag{5}$$

$$r_{RWGS} = \phi(1 - \phi)^{-1}k_3\left(p_{CO_2} - \frac{p_{CO}p_{H_2O}}{p_{H_2}K_{P3}}\right)\theta^\star\theta^\odot \tag{6}$$

with the reformulated Arrhenius equation

$$k_j = A_{k,j}\exp\left(-B_j\left(\frac{T_{ref}}{T} - 1\right)\right) \quad \text{with} \quad T_{ref} = 523.15\text{ K} \tag{7}$$

The corresponding surfaces are:

$$\theta^\odot = \left(1 + K_{CO}p_{CO} + K_{CH_3OH}^\odot p_{CH_3OH} + K_{CO_2}^\odot p_{CO_2}\right)^{-1} \tag{8}$$

$$\theta^\otimes = \left(1 + \sqrt{K_{H_2}p_{H_2}}\right)^{-1} \tag{9}$$

$$\theta^\star = \begin{pmatrix} 1 + K_{H_2O}p_{H_2O} + K_{CH_3OH}^* p_{CH_3OH} \\ +K_{CO_2}^* p_{CO_2} + \frac{K_{H_2O}K_O}{K_{H_2}}\frac{p_{H_2O}}{p_{H_2}} \end{pmatrix}^{-1} \tag{10}$$

Depending on the reducing/oxidizing potential of the reaction gas, oxidized sites are transformed reversibly into reduced sites and vice versa. This is described with an additional dynamic equation in the model [14, 15]:

$$\frac{d}{dt}\phi = k_1^+\left(y_{CO}(\phi_{max} - \phi) - \frac{1}{K_1}y_{CO_2}\phi\right) + k_2^+\left(y_{H_2}(\phi_{max} - \phi) - \frac{1}{K_2}y_{H_2O}\phi\right) \tag{11}$$

---

1)   List of symbols at the end of the paper.

The equilibrium constants can be expressed as function of free energies according to:

$$K_i = \frac{k_i^+}{k_i^-} = \exp\left(\frac{-\Delta G_i}{RT}\right) \tag{12}$$

The model describes with the parameters given in Tab. 1 the steady state and experimental data from [11] with good accuracy. A comparison with dynamic data will be discussed in Sect. 3.

2.2 Reactor Model

The focus of this paper is on analyzing the performance of a gradientless isothermal CSTR corresponding to the lab-scale micro Berty reactor described in [11]. Under these assumptions, the model equations follow from the overall material balances of the different species in both phases according to:

$$\frac{dn_i}{dt} = \frac{d}{dt}\left(n_i^G + n_i^S\right) = \dot{n}_0 y_{i,0} - \dot{n}y_i + m_{cat}\sum_j^{N_r} \nu_{i,j} r_j \tag{13}$$

with

$$n_i^G = y_i n^G \tag{14}$$

$$n_i^S = m_{cat} q_{sat} \Theta_i \tag{15}$$

Species to be considered are CH_3OH, CO_2, CO, H_2, H_2O, and N_2 for the cases with inert nitrogen. Assuming further a constant total pressure p, the molar outflow $\dot{n}$ follows from the overall material balances (see [18] for a detailed discussion). Process parameters used in this contribution are given in Tab. 2.

In these equations, the right-hand side reflects the rates of changes due to inflow, outflow, and chemical reaction. On the left-hand side, n_i^G and n_i^S represent the mole numbers of component i in the gas and the solid phase, respectively. y_i is

Table 2. Process parameters.

Parameter	Value	Units
p	60	[bar]
T	473	[K]
$y_{N_2,0,SS}$	0.15	[–]
F	0.114	[mL s^{-1}]
V^G	10.3	[mL]
m_{cat}	3.95	[g]
q_{sat}	0.98	[mmol g^{-1}]

the mole fraction of component i in the gas phase, and Θ_i is the total coverage of component i at the different active centers of the solid phase. As already mentioned in the previous section, adsorption equilibrium is assumed between the solid and the gas phase. Under these assumptions, the coverages Θ_i follow from the adsorption isotherms depending on the gas phase composition. Hereby, q_{sat} is the saturation adsorption capacity of the solid phase.

The evaluation of n_i^S in Eq. (13) requires careful consideration and is described in detail in [18]. The contribution of n_i^S on the left-hand side of the material balance (13) is often neglected and will be considered in some more detail in the remainder. Obviously, it does not play a role at steady state where the time derivative on the left-hand side is equal to zero. Therefore, it affects only the dynamics. The strength of this effect depends essentially on the saturation capacity q_{sat}. This effect is illustrated in Fig. 1 for different values of q_{sat} and compared to the dynamic experimental data from [11], where the carbon feed starts with a pure CO feed ($y_{CO} = 12.6\%$, $y_{H2} = 72.2\%$, and $y_{N2} = 16\%$) to establish an initial steady state.

After 140 min it is switched to pure CO_2 ($y_{CO2} = 11.9\%$, $y_{H2} = 71.5\%$, and $y_{N2} = 16.6\%$) again to pure CO at 210 min and back at 270 min. Constant conditions over the whole run

Table 1. Parameter values of the methanol kinetic model [16–18].

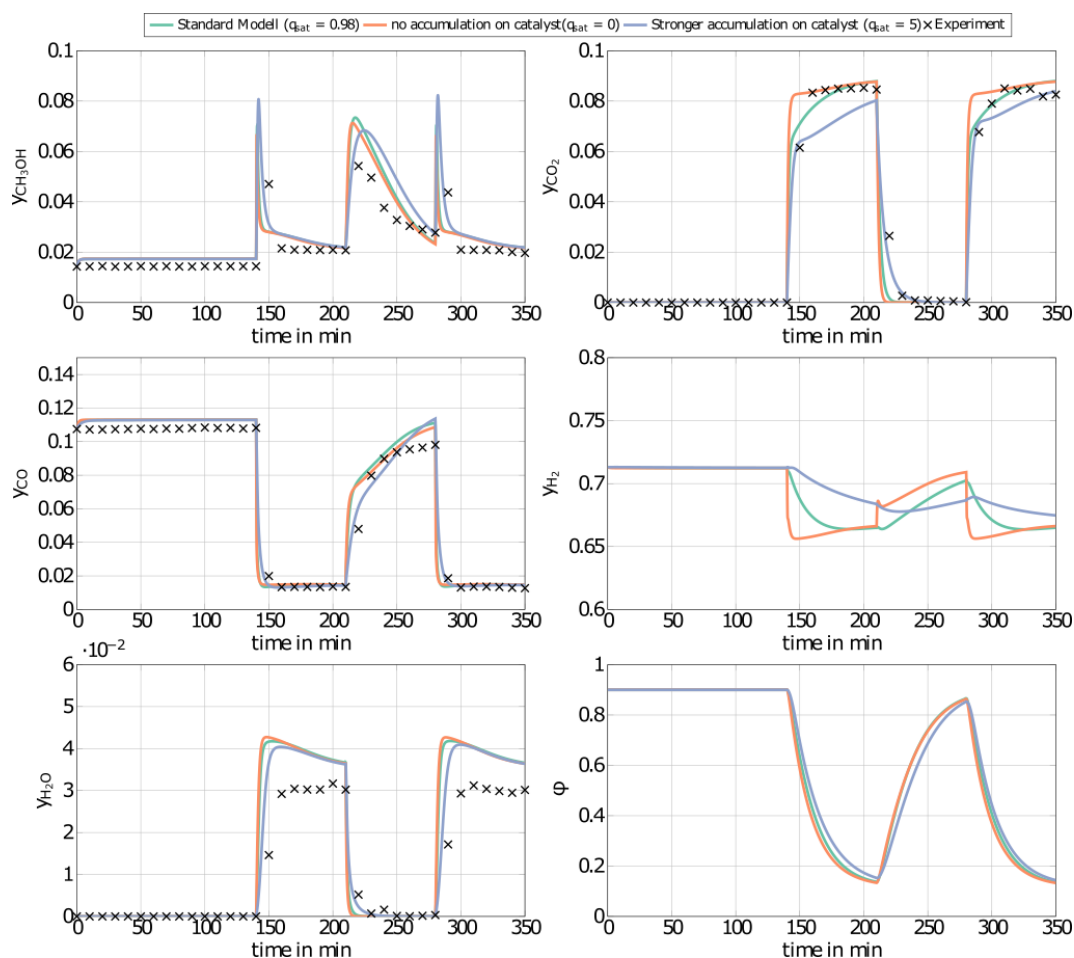| Parameter	Value	Units	Parameter	Value	Units
$A_{k,CO}$	0.00673	[mol s^{-1}kg$_{cat}^{-1}$bar^{-3}]	K_{CO}	0.1497	[bar^{-1}]
B_{CO}	26.4549	–	$K_{CH_3OH}^{\odot}$	0	[bar^{-1}]
A_{k,CO_2}	0.043	[mol s^{-1}kg$_{cat}^{-1}$bar^{-3}]	$K_{CO_2}^{\star}$	0.0629	[bar^{-1}]
B_{CO_2}	1.5308	–	$K_{CO_2}^{\odot}$	0	[bar^{-1}]
$A_{k,RWGS}$	0.0117	[mol s^{-1}kg$_{cat}^{-1}$bar^{-3}]	ΔG_1	0.3357×10^3	[J mol^{-1}]
B_{RWGS}	15.6154	–	ΔG_2	21.8414×10^3	[J mol^{-1}]
$\sqrt{K_{H_2}}$	1.1064	[bar$^{-1/2}$]	k_1^+	7.9174×10^3	[s^{-1}]
$K_{CH_3OH}^{\star}$	0	[bar^{-1}]	k_2^+	0.188×10^{-4}	[s^{-1}]
K_{H_2O}	0	[bar^{-1}]	ϕ_{max}	0.9	–
K_O	0	–			

Figure 1. Influence of the adsorption saturation capacity of the catalyst q_{sat} on the dynamic transient behavior. Comparison of model predictions for three different values of q_{sat} (solid lines) with experimental results from [11] (crosses). In these experiments 15 % of inert nitrogen was present in the feed.

are the temperature (T = 523 K), the pressure (50 bar), and the space velocity w.r.t the inlet flow (240 mL min^{-1}). In this figure, ϕ is the fraction of reduced centers on the catalyst surface [14,15]. If n_i^S is neglected (i.e., q_{sat} = 0 mol kg$_{cat}^{-1}$), the gas phase mole fractions change almost instantaneously in response to feed changes due to the small storage capacity of the gas phase. In contrast to this, for finite values of q_{sat} a significant lag is observed. A value of q_{sat} = 0.98 mol kg$_{cat}^{-1}$ was found to fit the experimental data best. For comparison also a storage value of q_{sat} = 5 mol kg$_{cat}^{-1}$, reflecting a catalyst material with very high storage capacity and therefore a slower response, is given. The effect of the saturation capacity on forced periodic operation will be further discussed below in Sect. 3.

2.3 Nonlinear Frequeny Response (NFR) Method

There are many ways of operating a system periodically, e.g., it is possible to periodically modulate different inputs or input combinations, using various forcing parameters, i.e., forcing frequency, input amplitude(s), and phase differences between the inputs. This richness of possible forcing strategies also

produces a challenge to find which forcing strategy is to be used in order to achieve the highest possible improvement (see, e.g., [5, 19–21]). One of the answers to this challenge is to apply the NFR method, which offers a systematic approach to the search for the best scenario. The NFR method is an approximate, but reliable analytical tool for evaluating possible improvements, which should be used in early stages of process development before rigorous numerical simulation and before experimental investigation [16, 17, 22].

The NFR method is a theoretical and powerful tool, mathematically based on Volterra series, generalized Fourier transforms, and the concept of higher-order frequency response functions (FRFs) [6, 22, 23]. In practice, the nonlinear model of the investigated system is replaced by a set of frequency response functions of different orders. The derivation procedure of these FRFs is standardized [24]. Although these analytical derivations can be tedious and time-consuming, especially for complex systems, the numerical burden associated with the application of the NFR method is practically negligible in comparison to classical numerical approaches. The recent introduction of a software application for automatic derivation of the FRFs, the so-called computer-aided nonlinear frequency

response (cNFR) method [25], substantially facilitates the derivation of the needed FRFs.

If one or more inputs of a weakly nonlinear systems is/are periodically modulated around a previously established steady state, the frequency response of the system output is a complex periodic function [26], obtained as a sum of the output steady-state value (y_s), the basis harmonic (y_I), an infinite number of higher harmonics (y_{II}, y_{III},…) and a non-periodic (DC) term (y_{DC}) [6, 22, 23]:

$$y(t) = y_s + y_{DC} + y_I + y_{II} + y_{III} + \ldots \quad (16)$$

Based on the NFR method, the change of the reactor performances caused by forced periodic operations can be evaluated from the non-periodic (the so-called DC) component of the frequency response of the reactor.

Using the concept of higher-order FRFs, the DC component can be written as the following infinite series [27]:

$$y_{DC} = 2\left(\frac{A}{2}\right)^2 G_{y,x,x}^{(2)}(\omega, -\omega)$$
$$+ 6\left(\frac{A}{2}\right)^4 G_{y,x,x,x,x}^{(4)}(\omega, \omega, -\omega, -\omega) + \ldots \quad (17)$$

In Eq. (17), $G_{y,x,x}^{(2)}(\omega, -\omega)$ is the asymmetrical second-order (ASO) FRF, $G_{y,x,x,x,x}^{(4)}(\omega, \omega, -\omega, -\omega)$ the asymmetrical fourth-order FRF, etc.

For weakly nonlinear systems, the significance of different terms in Eq. (17) decreases with the increase of the corresponding FRF order. As a consequence, the DC component can be approximated with its dominant term, which is proportional to the asymmetrical second-order function and the square of the input amplitude [6]:

$$y_{DC} \approx 2\left(\frac{A}{2}\right)^2 G_{y,x,x}^{(2)}(\omega, -\omega) \quad (18)$$

Eq. (18) is the foundation of the NFR method for evaluating periodic operations with one modulated input. Therefore, for single input modulations of, e.g., input x, the DC component is proportional to the second-order asymmetrical frequency response function (ASO FRF) $G_{y,x,x}^{(2)}(\omega, -\omega)$ relating the output of interest (y) and the modulated input (x), meaning that for single input forced periodically operated chemical reactors it is enough to derive and analyze only one FRF [16].

For simultaneous modulation of two inputs, the DC component is evaluated based on three FRFs, where two of them are correlating the output of interest to the two modulated inputs separately and one cross FRF which correlates the output to both modulated inputs. It should be pointed out that the cross effect of two inputs strongly depends on the phase shift of simultaneous modulation of those two inputs and that it is possible to achieve high improvement for simultaneous modulation of two inputs even for the cases when separate input modulations would not lead to improvement at all. The influence of the forcing parameters (frequency, amplitudes, and phase shift of the input modulations) on the possible improvement can also be determined by the NFR method [23].

The DC component of an output y, for the case when two inputs (e.g., x and z) are periodically modulated, can be given as a sum of the contributions of the DC component related to the single inputs (x and z) separately and the contribution of the DC component originating from the cross-effect of both inputs [7]:

$$y_{DC} = y_{DC,x} + y_{DC,z} + y_{DC,xz} \quad (19)$$

For co-sinusoidal modulations of inputs x and z, with equal frequencies ω, input amplitudes A_x and A_z, respectively, and phase difference φ between them, the separate contributions of the two inputs to the DC component can be approximately evaluated from the corresponding asymmetrical second-order FRFs, in the same way as explained above:

$$y_{DC,in} \approx 2\left(\frac{A_{in}}{2}\right)^2 G_{y,in,in}^{(2)}(\omega, -\omega) \text{ or } z \quad (20)$$

while the contribution of the cross-effect can be approximately evaluated in the following way [7, 23]:

$$y_{DC,xz} \approx 2\left(\frac{A_x}{2}\right)\left(\frac{A_z}{2}\right) G_{y,x,z}^{*(2)}(\omega, \varphi) \quad (21)$$

$G_{y,x,z}^{*(2)}(\omega, \varphi)$ is the so-called cross ASO term, which correlates the output y with both modulated inputs (x and z). It is a function of both frequency and phase difference between the two modulated inputs, and is evaluated based on the cross asymmetrical second-order FRF ($G_{y,x,z}^{(2)}(\omega, -\omega)$), in the following way:

$$G_{y,x,z}^{*(2)}(\omega, \varphi) = \cos(\varphi) Re\left(G_{y,x,z}^{(2)}(\omega, -\omega)\right)$$
$$+ \sin(\varphi) Im\left(G_{y,x,z}^{(2)}(\omega, -\omega)\right) \quad (22)$$

The overall DC component of the output y could be written as follows:

$$y_{DC} \approx 2\left(\frac{A_x}{2}\right)^2 G_{y,x,x}^{(2)}(\omega, -\omega) + 2\left(\frac{A_z}{2}\right)^2 G_{y,z,z}^{(2)}(\omega, -\omega)$$
$$+ 2\left(\frac{A_x}{2}\right)\left(\frac{A_z}{2}\right) G_{y,x,z}^{*(2)}(\omega, \varphi) \quad (23)$$

and should be calculated for a chosen set of forcing parameters (forcing frequency, forcing amplitudes, and phase difference) [7, 24]. In principle, it is possible to find a set of forcing parameters resulting the periodic operation with highest improvement [7, 23, 24].

The phase difference is a crucial parameter for a periodic operation with simultaneous modulations of two inputs, considering that by choosing the optimal phase difference the cross-effect can be maximized [7, 10, 23, 24].

Results for methanol synthesis specific for the gradientless isothermal, isobaric, lab-scale micro Berty reactor will be discussed in Sect. 3.

2.4 Optimization Methods

For a rigorous evaluation of the potential of forced periodic operation compared to conventional steady state operation, one should compare the best possible steady states with the

best possible forced periodic operation. This is done in this paper using multi-objective optimization. Objectives to be considered are the average methanol flow rate at the reactor outlet and methanol yield based on the total carbon feed.

$$J_1 = \dot{n}_{CH_3OH} \tag{24}$$

$$J_2 = \frac{\dot{n}_{CH_3OH}}{\dot{n}_{Carbon,in}} \tag{25}$$

The evaluation of the objective functions for the NFR method is given in the Appendix. For the computation of Pareto optimal steady- state and forced periodic solutions, a benchmark problem with given temperature, pressure, volume, average volumetric feed flow rate F, catalyst mass m_{cat} and, for Sect. 3.1, average inert nitrogen concentration in the feed $y_{N_2,0,SS}$ according to Tab. 2 is considered. The reactor dimension and the catalyst mass correspond to the experimental study of [11], which is the starting point for a parallel ongoing new experimental study.

In order to compute the Pareto front (see, e.g., Fig. 2 as an example), in a first step, two single objective optimization problems are solved to generate the left (maximum methanol flow rate) and the right (maximum methanol yield based on total carbon feed) boundary points of the Pareto front using a multi-start heuristic. In the second step, the Pareto front between these extreme points is traced out using the ε-constraint approach [8, 9] for multi-objective optimization as described in some more detail in [18] as follows:

$$\max_{x} J_1$$
$$s.t. \ J_2 \leq \varepsilon$$
$$\sum y_{i,0,SS} - 1 = 0$$
$$y_{CO,0,SS} + y_{CO_2,0,SS} \geq 0.01$$
$$\sum y(0) - 1 = 0 \tag{26}$$
$$y(0) = y(\tau)$$
$$\dot{V}_{out} > 0$$
with given ε from: $J_{2,min} \leq \varepsilon \leq J_{2,max}$

Here, the solution of the previous point is used as an initial guess for the current point. If the solver fails to converge, the calculation is redone by perturbing the initial values until convergence is achieved.

In contrast to [18], the underlying single objective optimization problems were solved using a simultaneous approach by discretizing the model in time using finite differences with 500 equidistant time steps per period.

Parameters to be optimized for steady-state optimization are the feed composition $y_{i,0,SS}$. Parameters to be optimized for forced periodic operation are the mean values in the feed $y_{i,0,SS}$, the forcing amplitudes of CO A_{CO} and the volumetric feed flow rate A_F, the forcing frequency ω, and the phase shift $\Delta\phi$ between the periodic forcing of the two inputs.

$$y_{CO,0}(t) = y_{CO,0,SS}(1 + A_{CO}\cos(\omega t)) \tag{27}$$

$$\dot{V}_0(t) = \dot{V}_{0,SS}(1 + A_F\cos(\omega t + \Delta\phi)) \tag{28}$$

For evaluating operation with an inert gas, the concentration of N₂ in the feed was also varied periodically in a countercur-
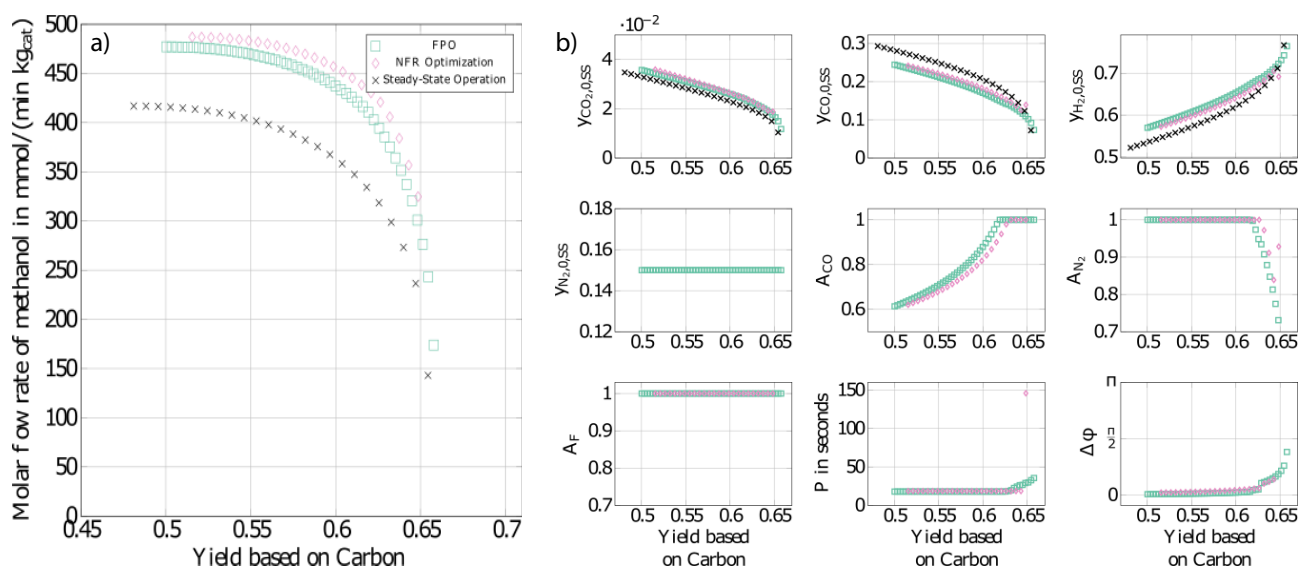

Figure 2. (a) Pareto fronts with inert nitrogen for steady-state operation (black crosses) compared to forced periodic operation as predicted by the multi-objective optimization of the full model (green boxes) and the NFR method (purple diamonds). (b) Corresponding optimal parameters values along the Pareto fronts in the upper diagram as a function of the yield based on total carbon in the feed. $y_{i,0,SS}$: average mole fraction of component i in the feed; A_{CO}, A_{N2}, A_F: amplitudes of input modulations of CO, N₂ and the outlet volumetric flow rate. P: periodic time, $\Delta\phi$: phase shift between input modulation of CO and F.

www.cet-journal.com

rent way to compensate the variation of CO and to meet the summation condition at any time t according to $\sum y_i(t) = 0$.

$$y_{N_2,0}(t) = y_{N_2,0,SS}\left(1 - A_{N_2}\cos(\omega t)\right)$$
with $A_{CO}y_{CO,0,SS} - A_{N_2}y_{N_2,0,SS} = 0$ (29)

For the industrially relevant operation without inert nitrogen this compensation was done by countercurrent periodic forcing of H_2.

It is important to note that the mean values $y_{i,0,SS}$ for forced periodic operation are also optimized and are therefore not identical with the corresponding values for steady-state optimization. For the optimization without inert nitrogen the constraint for $y_{H2,0,SS}$ is relaxed to $0.35 \leq y_{H2,0,SS} \leq 1$.

$$\begin{bmatrix} 0 \\ 0 \\ 0.5 \\ 0 \\ 0 \\ 0 \\ 18 \\ -\pi \\ 0 \end{bmatrix} \leq \begin{bmatrix} y_{CO,0,SS} \\ y_{CO_2,0,SS} \\ y_{H_2,0,SS} \\ A_F \\ A_{CO} \\ A_{N_2} \\ \tau \\ \Delta\phi \\ y_0 \end{bmatrix} \leq \begin{bmatrix} 1 \\ 1 \\ 0.85 \\ 1 \\ 1 \\ 1 \\ 3600 \\ \pi \\ 1 \end{bmatrix}$$ (30)

The single objective optimization problems were solved with Julia [28], applying the JuMP [29], a domain-specific modeling language for mathematical optimization. One of the major benefits of using JuMP is the capability of employing (forward mode) automatic differentiation (AD), which outperforms other (non-AD) algorithms in speed and accuracy [30]. The applied nonlinear solver is Ipopt 3.13.4.

In summary, it is found that the improved optimization methodology applied in this paper is much more robust and efficient than the methodology applied earlier in [18].

3 Results and Discussion

3.1 Optimization with Inert Nitrogen

Using first the NFR method it was found in preliminary studies that single input modulation does not provide potential for significant improvement of reactor performance in terms of the objectives (methanol flow rate and yield) introduced in the previous section [16]. The best potential for improvement was found for simultaneous modulation of the flow rate and the CO feed concentration [17]. Improvements of up to 33.51 % of methanol production (single objective) were reported and further studied with multi-objective optimization. The results of the approximate NFR method were validated with numerical simulation of the full blown model described above for selected operating points in [17].

Further comparison between multi-objective optimization with the NFR and the full model is depicted in Fig. 2 for the conditions described in [17]. In this figure, optimal steady-state operation is compared to optimal forced periodic operation as predicted by the two different approaches. Again, very good agreement between both approaches is found together with a significant potential for improvement of the methanol production rate in the left part of Fig. 2a. The periodic time required is about 18 s and the optimal phase shift between flow rate and CO inlet concentration is close to zero as shown in Fig. 2b. Consequently, there is periodic change between high CO feed flow rate, and afterwards the flow rate is reduced and CO is reacted away. In contrast to this, on the right side of the diagram (high yield region) not much improvement is found [17, 18].

In the remainder, results are extended step by step using numerical optimization of the full model. In a first step, a constraint on the volumetric outflow of the system is added. This is required since methanol synthesis is volume reducing and the feed flow rate at the input becomes zero at the minimum for large amplitudes of $A_F = 1$ in Fig. 2b. Results are presented in Fig. 3a.
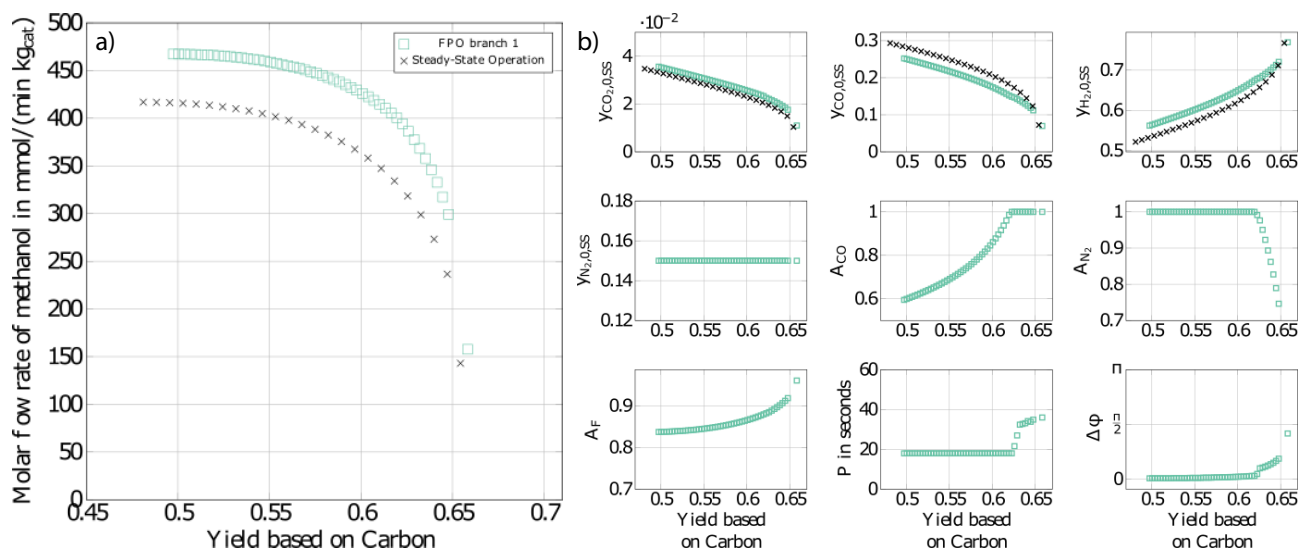

Figure 3. (a) Pareto fronts with inert nitrogen for steady-state operation (black crosses) compared to forced periodic operation as predicted by the multi-objective optimization of the full model (green boxes) with additional constraint on the outlet volumetric flow rate. (b) Corresponding parameter values. Nomenclature as described in Fig. 2.

At steady state, outlet volumetric flow rate non-negative was always satisfied, so that the steady-state Pareto front marked by the black crosses does not change. The effect on the Pareto front of forced periodic operation is also relatively small compared to the previous Fig. 2. Again, big improvements in terms of the methanol flow rate are found in the left part of Fig. 3, and minor improvements in the right part. Due to the additional constraint, improvements are reduced a little with a maximum reduction of about 2 % on the left side of the figure compared to Fig. 2. Due to the additional constraint of a non-negative outlet volumetric flow rate, the corresponding optimal forcing amplitude A_F is now restricted to values lower than 1 in Fig. 3b. The operating conditions in Fig. 3a essentially correspond to the base case which was considered in [18].

However, more recent calculations with the improved optimization methodology presented in this paper reveal that there exists an additional branch of the Pareto front which also predicts significant improvements compared to steady-state operation in the high yield part of the Pareto plot. This second branch is illustrated in Fig. 4a in red. The existence of the second branch of the Pareto front can be explained with the presence of multiple local minima of the present nonconvex optimization problem (see, e.g., [31]). Depending on the initial guesses either the green or the red branch in Fig. 4a is found.

After careful inspection using a refined multi-start approach no further branches were found. In principle, deterministic global optimization could be applied to prove that no better solutions exist than the red branch [31]. This, however, was not done due to the high computational effort. It is worth noting that the optimal forcing parameters along this second red branch are completely different from the previous green branch as shown in the diagram of Fig. 4b. In particular, the periodic time is now in the range of minutes with an increasing phase shift as we proceed to higher yields. Both branches merge at a yield of about 0.63.

For constant average inert nitrogen concentration applied so far, the total inert nitrogen feed flow rate as the product of total feed flow rate times concentration is not constant and in particular in the left part of Figs. 3 and 4 different from the steady-state value. Therefore, finally an additional constraint on the overall inert nitrogen feed flow as the product between the total flow rate and the concentration was added to the optimization problem and the assumption of constant average inert nitrogen concentration of $N_{N2,0,SS} = 0.15$ was relaxed.

$$\dot{\bar{n}}_{N_2,0} = \dot{n}_{N_2,0,SS} \qquad (31)$$

Results are illustrated as blue curves in Fig. 5 together with the branches from Fig. 4. It is shown that the potential for improvement in the right part of the diagram is even higher than the red curve, whereas the potential for improvement in the left part of the diagram is reduced. Periodic times are in the range of minutes, similar to the red branch. Phase shift in particular in the left part of the diagram is higher compared to the previous red and green curves. Improvements using forced periodic operation for chosen operating points can be found in Tab. 3.

Table 3. Results for operating points from Fig. 5a.

OP	$\dot{n}_{CH_3OH,SS}$	Y_{SS}	$\dot{n}_{CH_3OH,SS}$	Y_{FPO}
	[mmol min^{-1}kg$_{cat}^{-1}$]	[%]	[mmol min^{-1}kg$_{cat}^{-1}$]	[%]
OP1	347	61.1	370 (+6 %)	63.2 (+3.4 %)
OP2	236	64.7	316 (+34 %)	68.0 (+5.1 %)
OP3	143	65.4	298 (+108 %)	70.1 (+7.1 %)

3.2 Optimization without Inert Nitrogen

As mentioned above, the operating conditions considered in the previous section were inspired by the lab-scale experiments of [11]. In these experiments, the changing amounts of the inert nitrogen were used to quantify the contraction of the gas
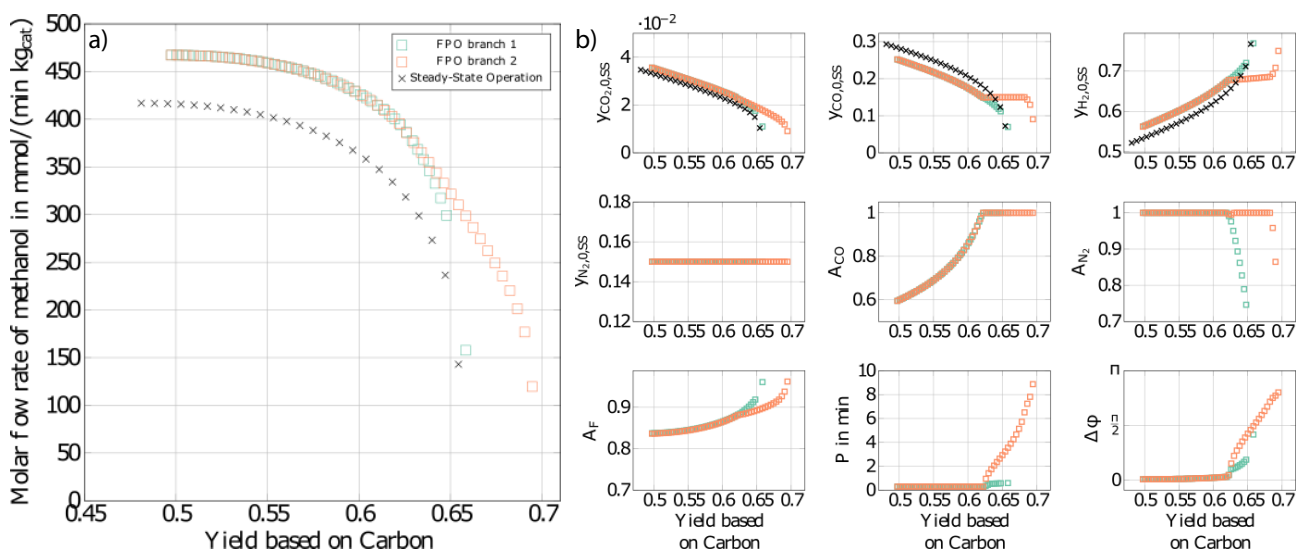

Figure 4. (a) Pareto fronts with inert nitrogen from Fig. 3 with additional branch in red. (b) Corresponding parameter values. Nomenclature as described in Fig. 2.
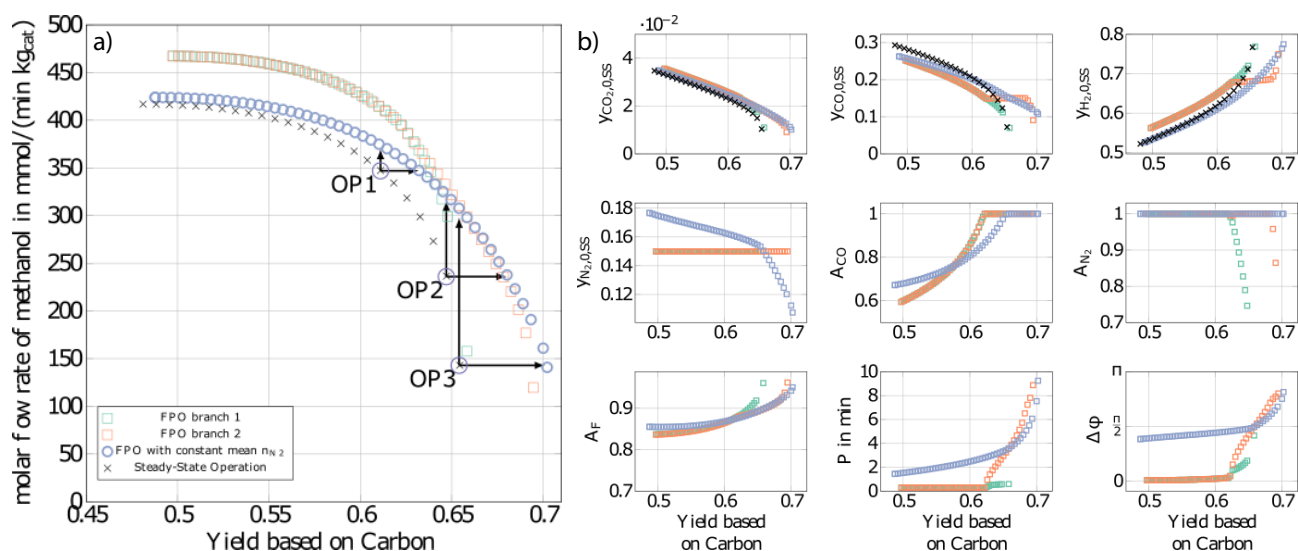
Figure 5. (a) Pareto fronts with inert nitrogen from Fig. 4 compared to the Pareto front with additional constraint for the average amount of inert in the feed (in blue). (b) Corresponding parameter values. Nomenclature as described in Fig. 2.

mixture due to the stoichiometry of the reactions. In industrial processes, however, depending on the source of the feed mixture, often only very little or no inert nitrogen is present [2, 4]. Therefore, the focus in this section is on optimal steady-state operation compared to optimal forced periodic operation without inert nitrogen in the feed. Again, periodic forcing of the CO feed concentration and the total volumetric feed flow rate is applied. To satisfy the closure condition at any time point, now H_2, instead of N_2, is used for compensation.

Results are illustrated in Fig. 6. In general, methanol production rates are higher for both, steady-state and forced periodic operation, due to more reactants in the feed than for the case with inert nitrogen discussed in the previous section. Most improvement is found in the high yield part of Fig. 6a. There, the methanol yield can be improved through forced periodic

operation for a given production rate, or the methanol flow rate for a given yield. The latter effect is particularly large in the high yield region. The methanol flow rate for the highest steady yield is almost doubled. Instead for low yields, in the left part of the diagram hardly any improvement is found. This situation is qualitatively similar to Fig. 5 with inert nitrogen and an additional constraint for the inert nitrogen feed flow rate. Again, the optimal periodic time is in the range of minutes and the optimal phase shift is in the range of $\pi/2$. Improvements using forced periodic operation for chosen operating points can be found in Tab. 4, which are in the some order of magnitude as the results with inert gas.

Further insight is provided by evaluating the corresponding average molar feed rates of the three different feed components in Fig. 7. Improvement of forced periodic operation is achieved,
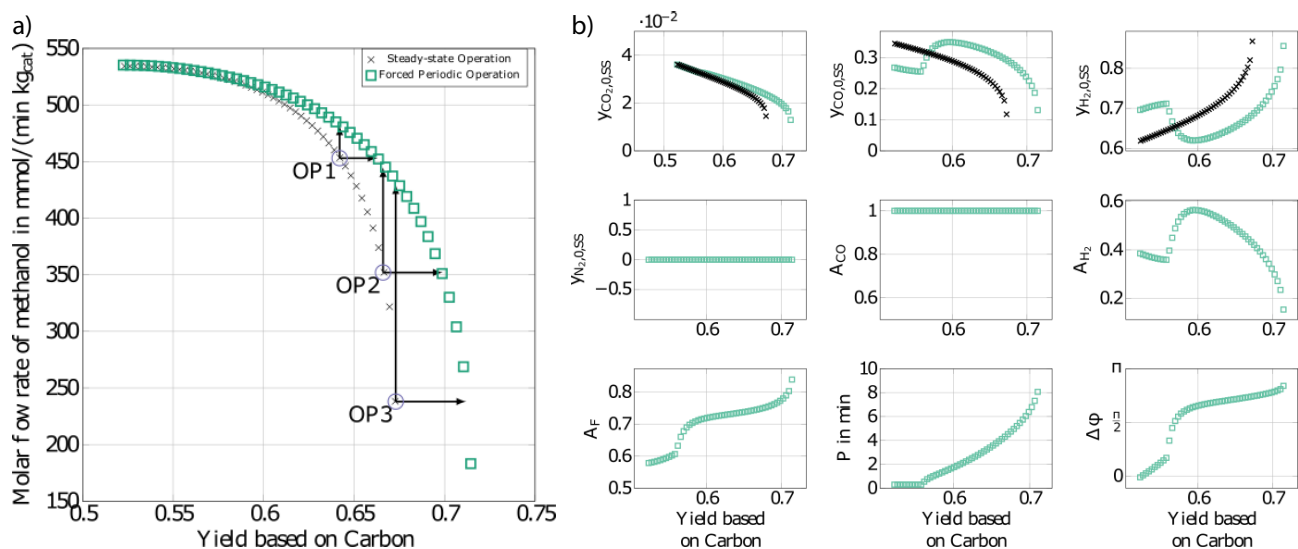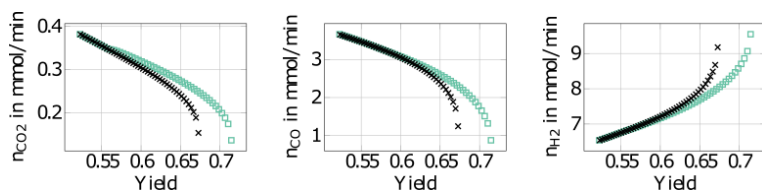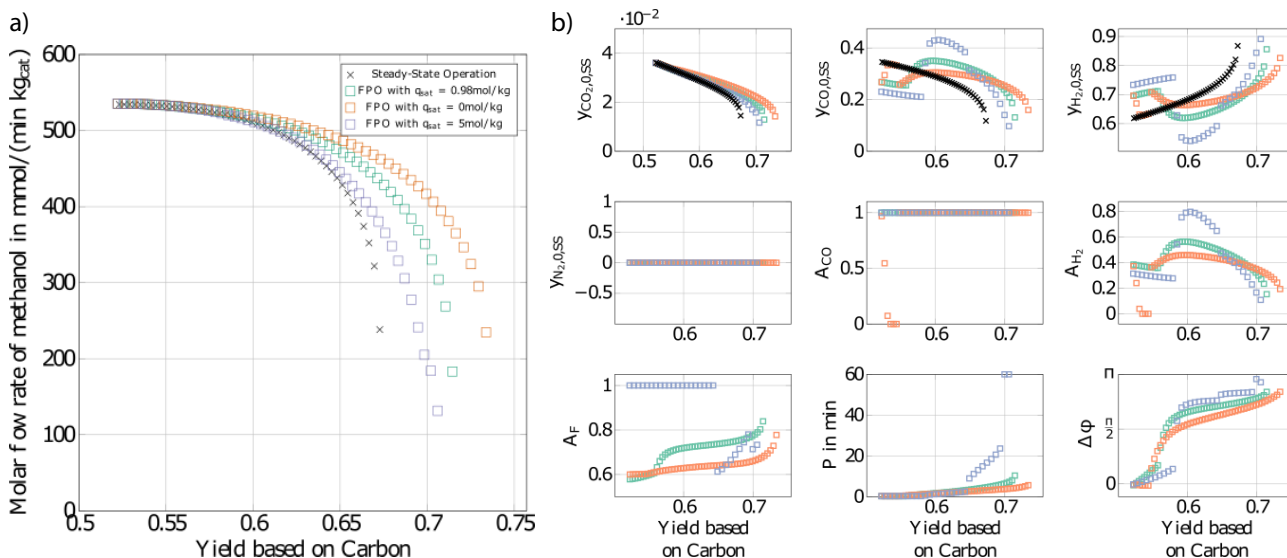

Figure 6. (a) Pareto fronts without inert nitrogen for steady-state operation (black crosses) compared to forced periodic operation (green boxes). (b) Corresponding parameter values. Nomenclature as described in Fig. 2.

Table 4. Results for operating points from Fig. 6a.

OP	$\dot{n}_{CH_3OH,SS}$	Y_{SS}	$\dot{n}_{CH_3OH,SS}$	Y_{FPO}
	[mmol min^{-1}kg$_{cat}^{-1}$]	[%]	[mmol min^{-1}kg$_{cat}^{-1}$]	[%]
OP1	453	64.2	482 (+6 %)	66.3 (+3.2 %)
OP2	352	66.6	445 (+26 %)	69.9 (+5 %)
OP3	238	67.3	430 (+80 %)	≈ 71.2 (+5.8 %)

with increased feed amounts of CO and CO_2 and a reduced amount of H_2. This seems to be particularly attractive for power-to-methanol processes (see, e.g., [1, 3, 32], where H_2 is generated via electrolysis with regenerative electrical energy and is therefore often more expensive. For the interpretation of the results it should be emphasized that both curves, i.e., the black for steady-state operation and the green for forced periodic operation, are optimal for the given objectives and constraints.

Finally, the effect of the saturation capacity of the catalyst q_{sat} on forced periodic operation is discussed. Results are presented in Fig. 8. As q_{sat} increases, the Pareto fronts of forced periodic operation tend towards the Pareto front of steady-state operation and improvements are getting smaller

and smaller. This is consistent with the observations in Sect. 2.2, where it was shown that a finite saturation capacity of the solid phase introduces an additional lag. Such a lag will lead to a dampening of the forced periodic solution bringing it closer to steady-state operation. Knowledge regarding the adsorption saturation capacity of the catalyst q_{sat} is therefore an important quantity for a reliable prediction of the potential for improvement through applying am optimized forced periodic operation. It appears to be essential to tune this catalyst property for an efficient periodic production of methanol.

4   Conclusion

Results of a theoretical study to exploit the potential of forced periodic operation for methanol synthesis are presented. Exploiting a validated kinetic model for a commercial Cu/Zn/Al$_2$O$_3$ catalyst, which captures essential dynamic features, it was demonstrated that for well-selected forcing parameters using optimized amplitudes, frequency, and phase shift significant improvements can be expected compared to conventionally applied steady-state operation.

The study was based on a powerful theoretical approach, combining nonlinear frequency response analysis with rigorous numerical multi-objective optimization of the full model. Results were presented for a gradientless isothermal CSTR operated under isobaric conditions with and without inert nitrogen in the feed. An increase of up to 108 % regarding the average molar flow rate of methanol and up to 7.2 % for the yield is predicted for the case with inert nitrogen. For the case without inert

Figure 7. Average feed rates of different components as a function of the yield based on carbon in the feed corresponding to the Pareto front without inert nitrogen in Fig. 6 for steady-state operation (black crosses) compared to forced periodic operation (green boxes).

Figure 8. (a) Pareto fronts without inert nitrogen for steady-state operation (black crosses) compared to forced periodic operation for different values of q_{sat}. Red boxes – q_{sat} = 0 mol kg^{-1}, green boxes – q_{sat} = 0.98 mol kg^{-1}, blue boxes – q_{sat} = 5 mol kg^{-1}. (b) Corresponding parameter values. Nomenclature as described in Fig. 2.

gas, improvements up to 80 % for the average molar flow rate and up to 5.8 % for the yield are possible. Future work will focus on the experimental validation of the findings and an extension to nonisothermal fixed-bed reactors as applied in industry.

Appendix

Objective Functions for NFR Method

Based on the NFR method, the change of objective functions which are defined in this paper (the outlet molar flow rate of methanol and yield of methanol based on total carbon) can be evaluated based on ASO FRFs and DC components of output of interest [16, 17].

Using the NFR method, the mean (time-average) value of the outlet molar flow rate of methanol, $(\dot{n}_{CH_3OH})_{mean}$, for simultaneous co-sinusoidal modulations of inputs x and z can be approximately calculated using the DC ASO FRFs throughout following expression:

$$(\dot{n}_{CH3OH})_{mean} \approx \dot{n}_{CH3OH,s}$$

$$\begin{pmatrix} 1 + 2\left(\dfrac{A_x}{2}\right)^2 H^{(2)}_{1,x,x}(\omega,-\omega) + 2\left(\dfrac{A_z}{2}\right)^2 \\ H^{(2)}_{1,z,z}(\omega,-\omega) + 2\left(\dfrac{A_x}{2}\right)\left(\dfrac{A_z}{2}\right) H^{*(2)}_{1,x,z}(\omega,\varphi) \end{pmatrix} \quad (32)$$

where $H^{(2)}_{1,x,x}(\omega,-\omega)$ and $H^{(2)}_{1,z,z}(\omega,-\omega)$ are the ASO FRFs frequency response functions which correlate the dimensionless outlet molar flow rate of methanol, separately, to modulated inputs x and z, respectively [16], while $H^{*(2)}_{1,x,z}(\omega,\varphi)$ is the cross ASO term which correlates the outlet molar flow-rate of methanol to both modulated inputs x and z [17].

$$\dot{n}_{CH_3OH,s} = \frac{(p_{CH_3OH}\dot{V})_s}{RT} \quad (33)$$

is the steady-state value of the outlet molar flow-rate of methanol. More details could be found in references [16] and [17].

Based on the mean value of the methanol outlet molar flow rate, two defined objective functions could be evaluated as follows:

– normalized methanol production per unit mass of catalyst:

$$\left(\dot{n}^{norm}_{CH_3OH}\right)_{FPO} = \frac{(\dot{n}_{CH_3OH})_{mean}}{m_{cat}} \quad (34)$$

– yield of methanol based of total carbon

$$\left(Y^{totC}_{CH_3OH}\right)_{FPO} = \frac{(\dot{n}_{CH3OH})_{mean}}{(\dot{n}_{CO2})_{0,s} + (\dot{n}_{CO})_{0,mean}} \quad (35)$$

Symbols used

A_x	[–]	amplitude of input of CO, N_2 or volumetric flow rate
F	[m³ s⁻¹]	volumetric flow rate
G	[–]	frequency response function
J	[–]	objective function
m_{cat}	[kg]	mass of catalyst
n	[mol]	molar amount
$\dot{n}$	[mol s⁻¹]	molar flow rate
p	[bar]	pressure
q_{sat}	[mol kg$_{cat}$⁻¹]	adsorption capacity
r	[mol s⁻¹kg$_{cat}$⁻¹]	rate of reaction
V^G	[m³]	volume of gas phase in the reactor
y	[–]	mole fraction

Greek letters

Θ	[–]	relative number of free surface centers
ϕ	[–]	fraction of reduced surface centers
$\Delta\phi$	[–]	phase shift calculated by numerical optimization
φ	[–]	phase shift calculated by NFR method
τ	[s]	period time
ω	[rad s⁻¹]	frequency

Subscripts

DC	non-periodic component of frequency response
SS	steady state
0	feed stream
i	component (i = 1 CH$_3$OH, i = 2 CO$_2$, i = 3 CO, i = 4 H$_2$, i = 5 H$_2$O, i = 6 N$_2$)
j	reaction (j = 1 CO hydrogenation, j = 2 CO$_2$ hydrogenation, j = 3 RWGS)
I,II,...	number of harmonics of the frequency response
x,y,z	inputs of the frequency response function (y = ouput of interest, x = input 1, z = input 2)

Superscripts

G	gas phase
S	solid phase
*	reduced surface center
⊙	oxidized surface center
⊗	heterolytic surface center

Abbreviations

AD	automatic differentiation
ASO	asymmetric second order
CSTR	continuous stirred-tank reactor
FPO	forced periodic operation
FRF	frequency response function
NFR	nonlinear frequency response
SS	steady state

References

[1] G. A. Olah, *Angew. Chem.* **2005**, *44 (18)*, 2636–2639. DOI: https://doi.org/10.1002/anie.200462121

[2] J. Ott, V. Gronemann, F. Pontzen, E. Fiedler, G. Grossmann, D. B. Kersebohm, G. Weiss, C. Witte, in *Ullmanns Encyclopedia of Industrial Chemistry*, Wiley-VCH, Weinheim **2012**. DOI: https://doi.org/10.1002/14356007

[3] K. Raeuchle, L. Plass, H.-J. Wernicke, M. Bertau, *Energy Technol.* **2016**, *4 (1)*, 193–200. DOI: https://doi.org/10.1002/ente.201500322

[4] F. Asinger, *Methanol - Chemie und Energierohstoff*, Springer, Berlin **1986**. DOI: https://doi.org/10.1007/978-3-642-70763-6_1

[5] *Periodic Operation of Reactors* (Eds: P. L. Silveston, R. R. Hudgins), Elsevier, Amsterdam **2013**. DOI: https://doi.org/10.1016/C2010-0-67302-0

[6] A. Marković, A.-S. Morgenstern, M. Petkovska, *Chem. Eng. Res. Des.* **2008**, *86 (7)*, 682–691. DOI: https://doi.org/10.1016/j.cherd.2008.02.003

[7] D. Nikolić Paunić, M. Petkovska, *Chem. Eng. Sci.* **2013**, *104*, 208–219. DOI: https://doi.org/10.1016/j.ces.2013.09.009

[8] M. Ehrgott, *Multicriteria Optimization*, 2nd ed., Springer Science & Media **2005**. DOI: https://doi.org/10.1007/3-540-27659-9

[9] R. T. Marler, J. S. Arora, *Struct. Multidiscip. Optim.* **2010**, *41*, 853–862. DOI: https://doi.org/10.1007/s00158-009-0460-7

[10] M. Felischak, L. Kaps, C. Hamel, D. Nikolić, M. Petkovska, A. Seidel-Morgenstern, *Chem. Eng. J.* **2021**, *410*, 128197. DOI: https://doi.org/10.1016/j.cej.2020.128197

[11] B. Vollbrecht, Zur Kinetik der Methanolsynthese an einem technischen Cu/ZnO/Al$_2$O$_3$-Katalysator, *Ph. D. Thesis*, Otto-von-Guericke University Magdeburg **2007**.

[12] J. M. Berty, *Chem. Eng. Prog.* **1974**, *70 (5)*, 78–85.

[13] J. M. Berty, *Experiments in Catalytic Reaction Engineering*, Vol. 124, Elsevier, New York **1999**.

[14] C. Seidel, A. Jörke, B. Vollbrecht, A. Seidel-Morgenstern, A. Kienle, *Chem. Eng. Sci.* **2018**, *175*, 130–138. DOI: https://doi.org/10.1016/j.ces.2017.09.043

[15] C. Seidel, A. Jörke, B. Vollbrecht, A. Seidel-Morgenstern, A. Kienle, *Chem. Eng. Sci.* **2020**, *223*, 115724. DOI: https://doi.org/10.1016/j.ces.2020.115724

[16] D. Nikolić, C. Seidel, M. Felischak, T. Milicić, A. Kienle, A. Seidel-Morgenstern, M. Petkovska, *Chem. Eng. Sci.* **2022**, *248, Part I*, 117134. DOI: https://doi.org/10.1016/j.ces.2021.117134

[17] D. Nikolić, C. Seidel, M. Felischak, T. Milicić, A. Kienle, A. Seidel-Morgenstern, M. Petkovska, *Chem. Eng. Sci.* **2022**, *248, Part II*, 117133. DOI: https://doi.org/10.1016/j.ces.2021.117133

[18] C. Seidel, D. Nikolić, M. Felischak, M. Petkovska, A. Seidel-Morgenstern, A. Kienle, *Processes* **2021**, *9 (5)*, 872. DOI: https://doi.org/10.3390/pr9050872

[19] C.-C. Chen, C. Hwang, R. Y. Yang, *Can. J. Chem. Eng.* **1994**, *72 (4)*, 672–682. DOI: https://doi.org/10.1002/cjce.5450720417

[20] P. Silveston, R. R. Hudgins, A. Renken, *Catal. Today* **1995**, *25 (2)*, 91–112. DOI: https://doi.org/10.1016/0920-5861(95)00101-K

[21] P. Silveston, *Composition Modulation of Catalytic Reactors*, Vol. 11, CRC Press, Boca Raton, FL **1998**. DOI: https://doi.org/10.1016/S0255-2701(99)00099-9

[22] M. Petkovska, A. Seidel-Morgenstern, in *Periodic Operation of Reactors* (Eds: P. L. Silveston, R. R. Hudgins), Elsevier, Amsterdam **2013**. DOI: https://doi.org/10.1016/C2010-0-67302-0

[23] M. Petkovska, D. Nikolić, A. Seidel-Morgenstern, *Israel J. Chem.* **2018**, *58*, 663–681. DOI: https://doi.org/10.1002/ijch.201700132

[24] D. Nikolić Paunić, Forced Periodically Operated Chemical Reactors-Evaluation and Analysis by the Nonlinear Frequency Response Method, *Ph. D. Thesis*, Faculty of Technology, Metallurgy, University Of Belgrade **2016**.

[25] L. A. Živković, T. Vidaković-Koch, M. Petkovska, *Processes* **2020**, *8 (11)*, 1354. DOI: https://doi.org/10.3390/pr8111354

[26] J. M. Douglas, *Process Dynamics and Control*, Prentice-Hall, Englewood Cliffs, NJ **1972**. DOI: https://doi.org/10.1002/aic.690180542

[27] *Sinusoidal Analysis and Modeling of Weakly Nonlinear Circuits* (Eds: D. D. Weiner, J. F. Spina), Van Nostrand Reinhold Company, New York **1980**.

[28] J. Bezanson, A. Edelman, S. Karpinski, V. B. Shah, *SIAM Rev.* **2017**, *59 (1)*, 65–98. DOI: https://doi.org/10.1137/141000671

[29] I. Dunning, J. Huchette, M. Lubin, *SIAM Rev.* **2017**, *59 (2)*, 295–320. DOI: https://doi.org/10.1137/15M1020575

[30] J. Revels, M. Lubin, T. Papamarkou, *arXiv:1607.07892 [cs.MS]* **2016**. DOI: https://doi.org/10.48550/arXiv.1607.07892

[31] *Global Optimization* (Eds: R. Horst, H. Tuy), Springer, Berlin **1993**. DOI: https://doi.org/10.1007/978-3-662-02598-7

[32] M. Martín, *Comput. Chem. Eng.* **2016**, *92*, 43–54. DOI: https://doi.org/10.1016/j.compchemeng.2016.05.001